© 2014. Published by The Company of Biologists Ltd | Journal of Cell Science (2014) 127, 4507–4517 doi:10.1242/jcs.156000

RESEARCH ARTICLE

Actin and PIP3 waves in giant cells reveal the inherent length scale of an excited state

Matthias Gerhardt[1], Mary Ecke[2], Michael Walz[1], Andreas Stengl[2], Carsten Beta[1] and Günther Gerisch[2,*]

ABSTRACT

The membrane and actin cortex of a motile cell can autonomously differentiate into two states, one typical of the front, the other of the tail. On the substrate-attached surface of *Dictyostelium discoideum* cells, dynamic patterns of front-like and tail-like states are generated that are well suited to monitor transitions between these states. To image large-scale pattern dynamics independently of boundary effects, we produced giant cells by electric-pulse-induced cell fusion. In these cells, actin waves are coupled to the front and back of phosphatidylinositol (3,4,5)-trisphosphate (PIP3)-rich bands that have a finite width. These composite waves propagate across the plasma membrane of the giant cells with undiminished velocity. After any disturbance, the bands of PIP3 return to their intrinsic width. Upon collision, the waves locally annihilate each other and change direction; at the cell border they are either extinguished or reflected. Accordingly, expanding areas of progressing PIP3 synthesis become unstable beyond a critical radius, their center switching from a front-like to a tail-like state. Our data suggest that PIP3 patterns in normal-sized cells are segments of the self-organizing patterns that evolve in giant cells.

KEY WORDS: Actin waves, PIP3 signals, Excitable systems, Cell polarity, Cell fusion

INTRODUCTION

Actin-based force generation is the principal mechanism of motility in eukaryotic cells. A signature of directional locomotion in many cell types is the polarization into well-defined front and tail regions that differ in terms of the composition and dynamics of the actin cytoskeleton and in the phosphoinositide signaling system of the membrane. In the front region, actin is polymerizing to drive the formation of membrane protrusions, whereas in the tail region, the cell body retracts owing to the contractile action of myosin II. The leading edge corresponds to a phosphatidylinositol (3,4,5)-trisphosphate (PIP3)-enriched membrane at the cell front. The front is distinguished from the back of the cell, which is dominated by the PIP3-degrading phosphatase PTEN (Funamoto et al., 2002; Iijima and Devreotes, 2002). Front- and tail-type regions can also self-organize into dynamic patterns on the planar lower surface of a cell, where transition zones between the two states travel along the substrate-attached membrane (Arai et al., 2010; Schroth-Diez et al., 2009; Shibata et al., 2012; Taniguchi et al., 2013). These zones are decorated with an actin-rich band, called an actin wave.

An overview of various types of actin-based waves has been provided by Allard and Mogilner (Allard and Mogilner, 2013). The actin waves studied by us in *Dictyostelium discoideum* cells differ in principle from waves that are produced in an *in vitro* motility assay by instabilities in the myosin-driven translocation of pre-established actin filaments (Schaller et al., 2010). As revealed by fluorescence recovery after photobleaching (FRAP), the actin waves in *Dictyostelium* travel by the net polymerization of actin at their front and net depolymerization at their back (Bretschneider et al., 2009). Similarly, waves of Hem-1 (also known as NCKAP1L), a subunit of the WAVE complex that promotes Arp2/3-mediated actin polymerization, propagate by the recruitment of Hem-1 at their front and its release at their back (Weiner et al., 2007). In human osteosarcoma cells, ventral actin waves can generate transmembrane signals by integrin activation (Case and Waterman, 2011). These adhesive waves are associated with the Arp2/3 complex, as are the actin waves in *Dictyostelium*.

No membrane folds have been detected beneath the actin waves on the substrate-attached surface of *Dictyostelium* cells (Gerisch et al., 2004). The planar membrane on which these waves are traveling distinguishes them from circular dorsal ruffles, which are shaped by curved proteins that bind to convex or concave portions of the membrane, where they activate the polymerization of actin (Peleg et al., 2011).

Actin waves on a planar substrate-attached cell surface are not necessarily associated with cell movement or changes in cell shape, and thus differ from waves that reflect spatiotemporal patterns in the protrusive activity of a motile cell. The latter class of waves comprises periodic actin-based protrusions in various mouse and *Drosophila* cells (Döbereiner et al., 2006), and curvature waves in *Dictyostelium* that travel from the leading edge to the tail of a cell (Driscoll et al., 2012).

The actin waves propagating on the substrate-attached surface of *Dictyostelium* cells are supposed to be instrumental in the search for bacteria to be taken up by phagocytosis (Gerisch et al., 2009). These waves typically display a closed, ring-shaped structure and circumscribe a PIP3-rich inner territory that differs from an external area decorated with PTEN, a PIP3-degrading phosphoinositide 3 (PI3) phosphatase. Several criteria relate the inner territory to the front and the external area to the tail region of a polarized cell. The membrane of the inner territory is distinguished not only by the enrichment in PIP3 and the lack of PTEN, but also by the activation of Ras (Gerisch et al., 2011). Correlated with differences in the membrane are differences in the structure and composition of the underlying actin network – the inner territory of densely packed actin filaments is enriched in the Arp2/3 complex, whereas the external area consists of wide-meshed actin bundles that are associated with myosin-II and the

[1]University Potsdam, Institute of Physics and Astronomy, 14476 Potsdam-Golm, Germany. [2]Max Planck Institute of Biochemistry, 82152 Martinsried, Germany.

*Author for correspondence (gerisch@biochem.mpg.de)

Received 2 May 2014; Accepted 25 July 2014

Journal of Cell Science (2014) 127, 4507–4517 doi:10.1242/jcs.156000

actin-bundling protein cortexillin (Schroth-Diez et al., 2009). Thus, the wave patterns on the substrate-attached cell surface provide an opportunity to image, within one plane of focus, transitions between two states of the cell membrane in line with changes in the underlying actin cortex (Gerisch et al., 2012).

Excitability of the membrane and cortical actin layer has been implicated in the periodicity of actin polymerization at the leading edge (Ryan et al., 2012) and in the chemotaxis of eukaryotic cells (Shi and Iglesias, 2013; Nishikawa et al., 2014). The wave dynamics in *Dictyostelium* provide a system to study the propagation of an excited state within a single cell (Gerisch et al., 2012). The wave patterns that have been previously analyzed were formed within the boundaries of a single cell where the lateral borders confined the space for wave expansion to 10–20 µm, allowing only sections of the pattern to develop. To eliminate these restrictions of pattern development, we used cells in which the total membrane area is greatly enlarged such that the cell borders are far off.

Giant cells were either produced by cultivating myosin-II-deficient cells in suspension where the mutant cells are unable to divide (DeLozanne and Spudich, 1987; Knecht and Loomis, 1987) or they were generated in a wild-type background by electric-pulse-induced cell fusion (Gerisch et al., 2013). The giant cells enabled us to investigate the unpinned and undampened propagation of actin waves over distances that exceeded the radius of a normal cell by an order of magnitude. Here, we demonstrate that PIP3 patterns self-organize into dynamic zones with an intrinsic length scale. Independent of cell size, this length scale determines the distance between leading and trailing actin waves that are coupled to the borders of the PIP3-rich territories.

RESULTS

Dictyostelium cells fused by electric pulses form an intact actin cortex that supports long-range wave propagation

To monitor actin waves on the substrate-attached surface of giant cells, we fused cells that expressed markers for both the front and tail region of a normal motile cell – mRFP–LimEΔ, a label for filamentous actin that is enriched at the front of the cell (Fischer et al., 2004) and GFP–myosin-II heavy chain, a marker for the tail region (Moores et al., 1996). The electrofused cell shown in Fig. 1 exemplifies three features that are typical of the wave patterns in giant cells: (1) the waves can propagate with undiminished velocity over long distances, largely undisturbed by the cell boundary; (2) when waves collide, they tend to extinguish each other; and (3) there is no persistent pacemaker that serves as the origin of a periodic wave pattern. In this large cell, a zone enriched in myosin II was formed at an average distance of 6 µm behind the peak of the actin wave, independently of the cell border.

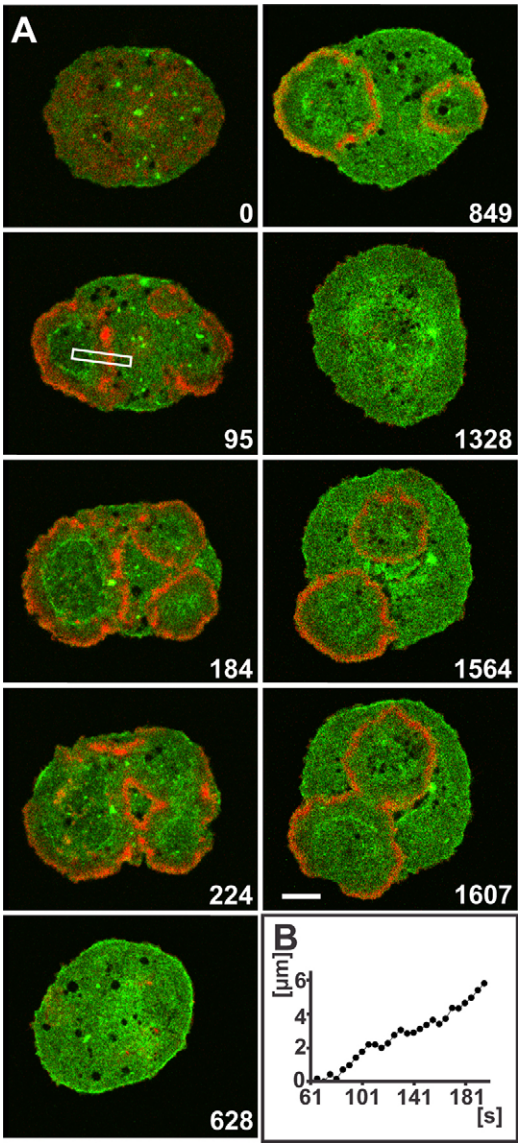

Fig. 1. Propagation of actin waves followed by myosin-II enriched zones. (A) Development of a wave pattern in an electrofused cell expressing mRFP–LimEΔ as a label for filamentous actin (red) and GFP–myosin-II heavy chains (green). The confocal images show the substrate-attached cell surface. The left panel begins with indistinct actin clustering throughout the entire surface area (0 s), and ends with the fusion and extinction of three actin waves (224–628 s). Myosin II assembles into filaments preferentially in a zone traveling behind the actin waves. The right panel begins with the re-start of wave formation (849 s), continues with extinction of the wave (1328 s), and ends with a second re-start at new sites of origin (1564–1607 s). Numbers indicate seconds after the first frame. Scale bar, 10 µm. (B) Plot of wave propagation obtained by recording the movement of the actin peak along the scan area indicated in the 95 s frame of A.

Features of actin patterns in giant cells

A variety of wave patterns in giant cells is illustrated in Fig. 2, showing a large myosin-II-null cell that expressed LimEΔ–GFP as a label for filamentous actin. Dominant features of the patterns are actin-enriched bands with peaks of actin accumulation at their border (Fig. 2A). These bands are polarized and mobile. They propagate across the substrate-attached surface of the cell with one of their broadsides ahead with an average velocity of 0.12 µm×s^{-1}±0.06 (±s.d.). The actin-rich border of the band corresponds to the actin waves previously studied in normal-sized cells (Gerisch et al., 2011). In the giant cells, these waves consist of a leading and a trailing segment (Fig. 2B; supplementary material Movie 1). In accordance with the terms employed for normal-sized cells, we designate the band-shaped regions surrounded by the actin waves as ‘inner territory’ and the regions outside the wave as ‘external area’ (Gerisch et al., 2011). In normal-sized cells, the inner territory has been shown to be enriched in the Arp2/3 complex, the external area to be associated with myosin II (Schroth-Diez et al., 2009).

Typically, pattern formation begins with the local clustering of actin, followed by the circular spreading of a wave from the

Journal of Cell Science (2014) 127, 4507–4517 doi:10.1242/jcs.156000

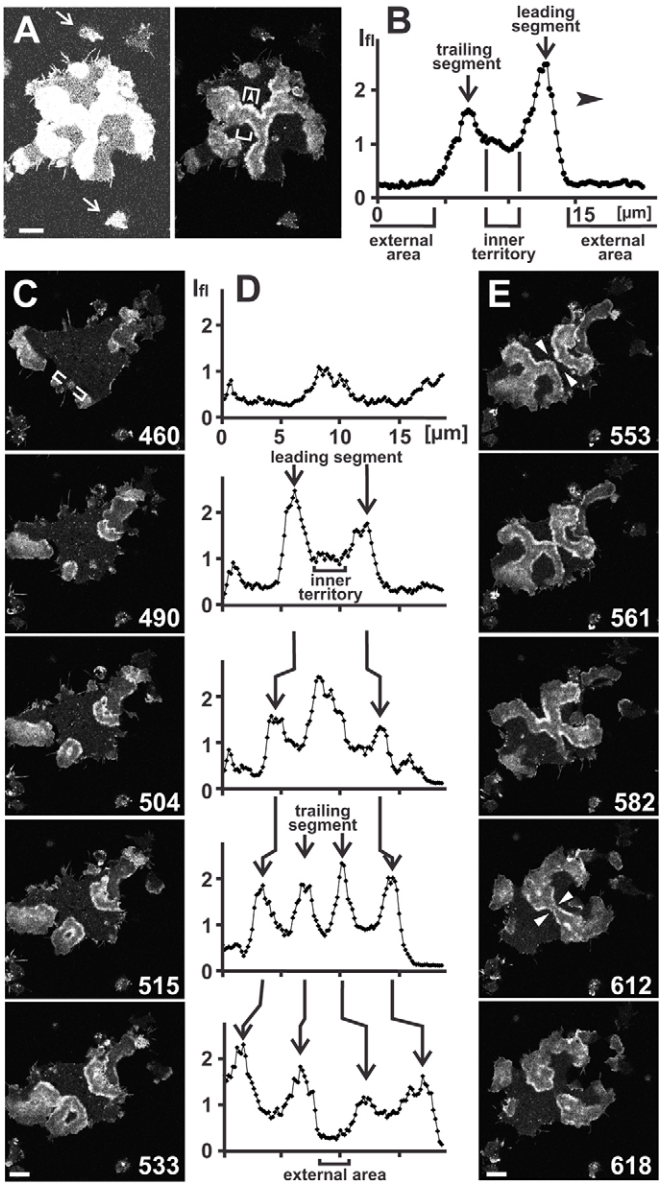

Fig. 2. Patterns of actin waves in a large myosin-II-null cell that expressed LimEΔ–GFP as a label for filamentous actin. Fluorescence images are focused on the substrate-attached cell surface where the wave patterns are formed. (A) Overview of an actin pattern. The left image is overexposed to visualize the shape of the cell with actin-rich filopodia on its border and the typical arrangement of filamentous actin in branched bands. The right image, at lower exposure, highlights the actin waves at the border of the bands by their prominent accumulation of filamentous actin. These waves envelop an 'inner territory' covered with a dense texture of actin filaments, and are surrounded by an 'external area' that contains a loose actin network. Arrows point to two normal-sized cells. (B) Fluorescence intensities (I_{fl}) in arbitrary units, scanned across an actin band as indicated in the right panel of A. Movement of the actin band in the direction of the arrowheads in A and B distinguishes a leading segment from a trailing one. Because of the dense texture of the actin network in the inner territory between these segments, the fluorescence intensity of the actin label is higher in this territory than in the external area. (C) Images of a time-series from the cell shown in A. The images illustrate the initiation and propagation of an actin wave, followed by insertion of a trailing wave. (D) Scans of fluorescence intensities corresponding to the images in C. The position of the scans are indicated in the first panel of C. The scans show the initiation and propagation of leading and trailing waves. The actin label drops when inner territory turns into external area. (E) Time-series showing the fusion of two wave systems followed by splitting. Both events are indicated by arrowheads. This sequence is a continuation of the one shown in C. The entire recording is documented in supplementary material Movie 1. Numbers in the frames of C and E designate seconds in accord with frame numbers of the movie. Scale bars, 10 μm.

initiation site (Fig. 2C,D). The concentric pattern eventually breaks and gives rise to waves that continue to propagate as actin-rich bands in radial direction (Fig. 2E, 553 and 561 s frames). When the bands collide, they extinguish each other locally followed by their fusion, as shown in Fig. 2E (582 to 618 s frames) and in supplementary material Movie 1.

Expanding waves maintain a constant width

The overview of shape dynamics shown in Fig. 2 and supplementary material Movie 1 reveals a preference for band-shaped waves with a preserved width. To substantiate this observation, we have developed an image-processing tool to represent the wave width and its changes over time. If a pattern is dominated by a specific width this will produce a peak in the distribution plot. The evolution of a dominant width is reflected in changing positions of the most prominent peak as a function of time. This analysis is illustrated in Fig. 3A–D for two scenarios, the expansion of a circular wave and the propagation of a band-shaped wave.

The actin wave shown in Fig. 3A undergoes expansion until, at a critical size, a circular trailing wave is inserted that leads to a 'doughnut' pattern. In the evolution of the width distribution, the circular expansion is reflected in a gradual shift of the dominant peak to larger values, until at 48 s the preferred width of ~12 μm is restored by the emerging doughnut shape (Fig. 3E).

The width of the wave displayed in Fig. 3B and supplementary material Movie 2 stays constant at about 15 μm for >5 min until, after 400 s, a segment of the wave widens, resulting in a second peak in the distribution that gradually shifts to larger values (Fig. 3F). After 470 s, the widened area is converted into an arc-shaped structure and the distribution returns to a single peak between 10 and 15 μm. The overview of supplementary material Movie 3 adds further examples for relaxation of the system into that preferred width between the outer borders of the actin wave. In conclusion, a key principle of the wave pattern is an inherent length scale that does not vary with cell size.

PIP3 dynamics in the wave patterns of giant cells

The territory enclosed by the leading and trailing segments of an actin wave propagates as a coherent PIP3-enriched band (Fig. 4A,B; supplementary material Movie 4). To explore the PIP3 dynamics during wave propagation, we measured the fluorescence intensities of the marker GFP–PHcrac (Parent and Devreotes, 1999) at multiple points on the substrate-attached surface of giant cells. For an unbiased sampling of temporal changes in a field of PIP3 waves, points of measurement were distributed on a rectangular grid with a distance of 10 μm between the points (Fig. 4C). This is about the diameter of a non-fused normal-sized cell. At each site, the passage of a wave produced a transient increase in PIP3. As an example, the time-series obtained at the point encircled in Fig. 4C is displayed in Fig. 4D. The distribution of peak-to-peak intervals extends over a wide range, suggesting that the system did not oscillate at a specific frequency (Fig. 4E).

Journal of Cell Science (2014) 127, 4507–4517 doi:10.1242/jcs.156000

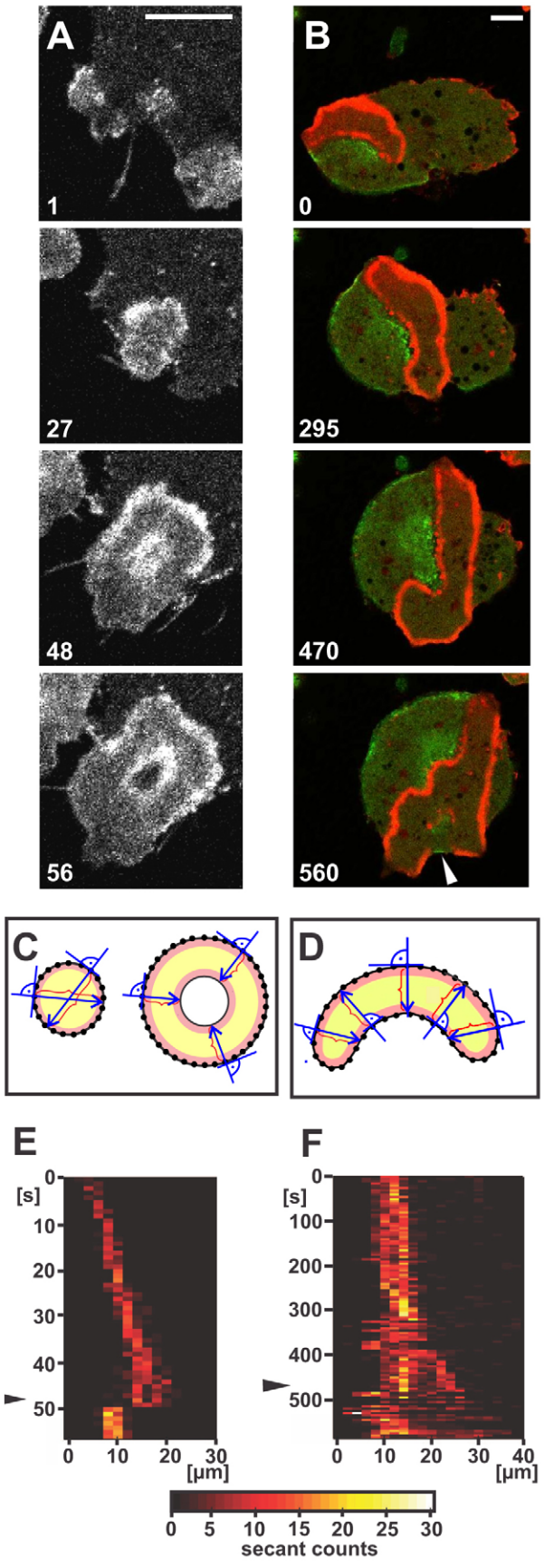

Fig. 3. Quantitative analysis of the shape of actin waves. (A) Sequence of images depicting the insertion of a trailing wave during the expansion of a circular actin wave in a large myosin-II-null cell. (B) Images displaying the dynamics of a band-shaped actin wave (red) in a large cell obtained by electrofusion. The cell also expressed GFP–myosin-II heavy chains (green). The arrowhead in the 560-s frame points to an arc-shaped indentation where internal area, surrounded by the wave, is converted to external area. Time in A and B is indicated in seconds in accord with E and F. Image 1 in A corresponds to the 460-s image of Fig. 2C. Scale bars: 10 µm. The full image series for B is shown in supplementary material Movie 2. (C,D) Measuring the width of actin waves. For an expanding circular wave (C) or a band-shaped traveling wave (D), the dominant width was computed by approximating the wave by a polygon. At each point of the contour, the width was calculated by taking the distance to the opposite side in a direction normal to the contour at the point of interest (arrows). Then the probability distribution of the wave width was computed for each time point. (E,F) Time-series from top to bottom of probability distributions for the waves shown in A and B, respectively. The insertion of a trailing wave seen in the 48-s frame is reflected in a switch of the distribution to smaller values (arrowhead in E). The local expansion of the wave seen in the 470-s frame of B is reflected in a branching of the distribution (arrowhead in F). Frequencies of the wave widths are color-coded as illustrated in the horizontal bar on the bottom.

Among the transient PIP3 increases, we selected those corresponding to waves that were not influenced by the cell border or by interference with another wave. Averaging the scans shown in Fig. 4F resulted in a curve with a width at half-maximum of 44 s. A rise time of 17 s from half-maximum to maximum and a slower decay of 27 s from maximum down to half-maximum results in an asymmetric shape of the temporal PIP3 profile. No extended plateau of PIP3 accumulation was observed. The spatial profile of PIP3 normal to the direction of wave propagation is shown in Fig. 4G. This profile is characterized by a distance from half-maximum to maximum of 2.1 µm, and a distance from maximum back to half-maximum of 3.0 µm. The mean velocity of propagation was 0.13 µm×s^{-1}±0.03 (±s.d.).

Inner territory converts to external area when a trailing wave is inserted

As shown in Fig. 4F,G, the PIP3 increase during the passage of a band-shaped wave across a point of the cell surface has a limited lifetime of ~44 s and a width in space of 5 µm at half-maximum. This pattern evolves from circular waves that radially expand from their site of origin, as shown for an early stage of pattern formation in Fig. 1. If the lifetime of the PIP3-rich state of the membrane is limited, there should be a critical radius, beyond which the territory within a circular wave becomes unstable such that its center will turn from the PIP3-rich into a PIP3-depleted state. Fig. 5 shows three examples of how the conversion of a circular PIP3 pattern into a propagating band pattern takes place. In the case of Fig. 5A, also shown in supplementary material Movie 5, the circular area is almost symmetrically divided into two bands by the lateral ingression of external area from two opposite sides. The measurement of PIP3 dynamics at different points in the field indicates a change from longer to shorter persistence times during evolution of the circular area into propagating bands (Fig. 5B). It appears, therefore, that during expansion of a circular wave, PIP3 is in a metastable state, before it relaxes into the steady state of synthesis and degradation that dominates the band pattern of PIP3 in giant cells. Often the external area ingresses only from one side, converting the circular PIP3-rich area into a horseshoe-shaped band with two open ends.

Journal of Cell Science (2014) 127, 4507–4517 doi:10.1242/jcs.156000

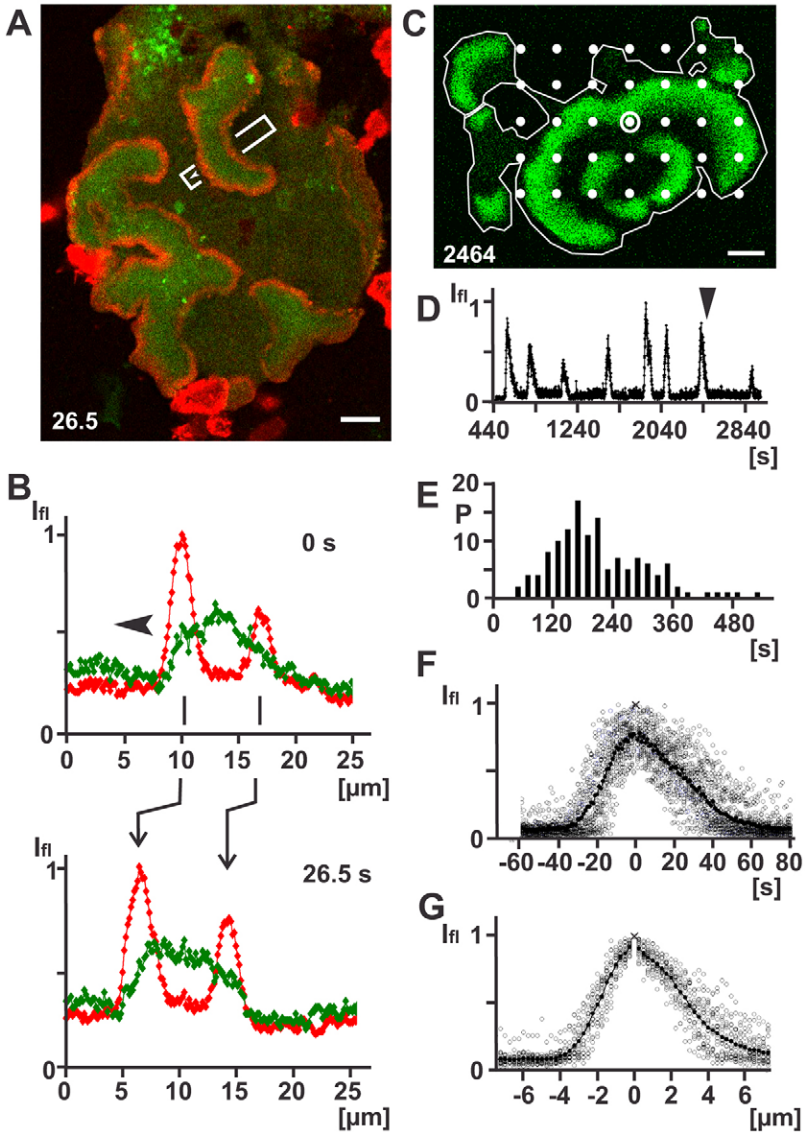

Fig. 4. PIP3 dynamics associated with actin waves. (A) An electrofused cell labeled for PIP3 with GFP–PHcrac (green) and for filamentous actin with mRFP–LimEΔ (red). The arrowhead on the bar points into the direction of wave propagation. (B) Fluorescence intensities (I_{fl}) scanned along the bar shown in A at 0 s (upper panel) and 26.5 s later (lower panel), the time at which the image of A was taken. The arrowhead in the 0-s frame indicates the direction of propagation of the combined PIP3 and actin wave. (C) PIP3 pattern in an electrofused cell used for the analysis of PIP3 dynamics. The cell changed shape during the recording as shown in supplementary material Movie 4. The actual perimeter at the 2464-s frame of the movie is indicated by a white line. The array of white dots demarcates points of measurement. (D) Temporal pattern of fluorescence intensities at the dot circled in C. The time at which the image of C was acquired is indicated by an arrowhead. (E) Probability distribution (P) of the time intervals between PIP3 peaks, compiled from 138 measurements in time-series like the one shown in D. (F) Temporal profile of PIP3 during the passage of a wave over single points of the array shown in C, displayed as the mean of 23 measurements. (G) Spatial profile of PIP3 in the direction of wave propagation, shown as the mean of 22 scans at different positions of the cell membrane. The scans are adjusted and normalized to the points of highest fluorescence intensity. Scale bars: 10 µm.

The two cases shown in Fig. 5C,D are distinguished by a prolonged preservation of symmetry. Here, the coherent PIP3-rich area is transformed into a 'doughnut' pattern consisting of a PIP3-rich annulus and a PIP3-depleted area in the center of the doughnut (Fig. 5C; supplementary material Movie 6). During the decline of PIP3 in this area, a circular actin wave is inserted. To provide evidence that the PIP3-depleted area changes its specification, we have co-labeled cells with GFP–myosin-II heavy chains. This label indicates that filamentous myosin II strongly assembles in the central area of a doughnut pattern, thus underscoring the transition from a front-like into a tail-like state (Fig. 5D; supplementary material Movie 7). The preference for band patterns with a defined width is also maintained during splitting, curling and budding of PIP3-rich territories. In particular, lateral expansion contributes to the elongated shape of the bands (supplementary material Fig. S1).

Variability of refractory phases

In an excitable system, a period of stimulation is typically followed by a refractory phase during which a stimulus cannot evoke a second response. The unidirectional propagation of PIP3 waves suggests that, after a period of activation, the PI3 kinases pass a state of refractoriness. Moreover, when two waves collide, they most often extinguish each other, as shown in Fig. 2E and supplementary material Movies 4, 8. This behavior is typical of waves in an excitable system that are followed by a refractory phase. Nevertheless, a detailed analysis of pattern dynamics in giant cells indicated that the refractory phase can be short, and an absolute refractoriness is sometimes lacking. In the giant cells, we investigated the variability of refractory phases using waves that collide with the cell border.

Frequently, waves disappeared from the substrate-attached cell surface after collision with the cell border, as expected if excitation is followed by a refractory phase (Fig. 6A,B). In other cases, the waves were not completely extinguished at the border of the cell; remnants persisted and propagated backward along the substrate-attached cell membrane. In these remnants of a wave, PIP3 remained at a high level for a longer period of time than during unperturbed wave propagation (Fig. 6C,D as compared to Fig. 4F).

Journal of Cell Science (2014) 127, 4507–4517 doi:10.1242/jcs.156000

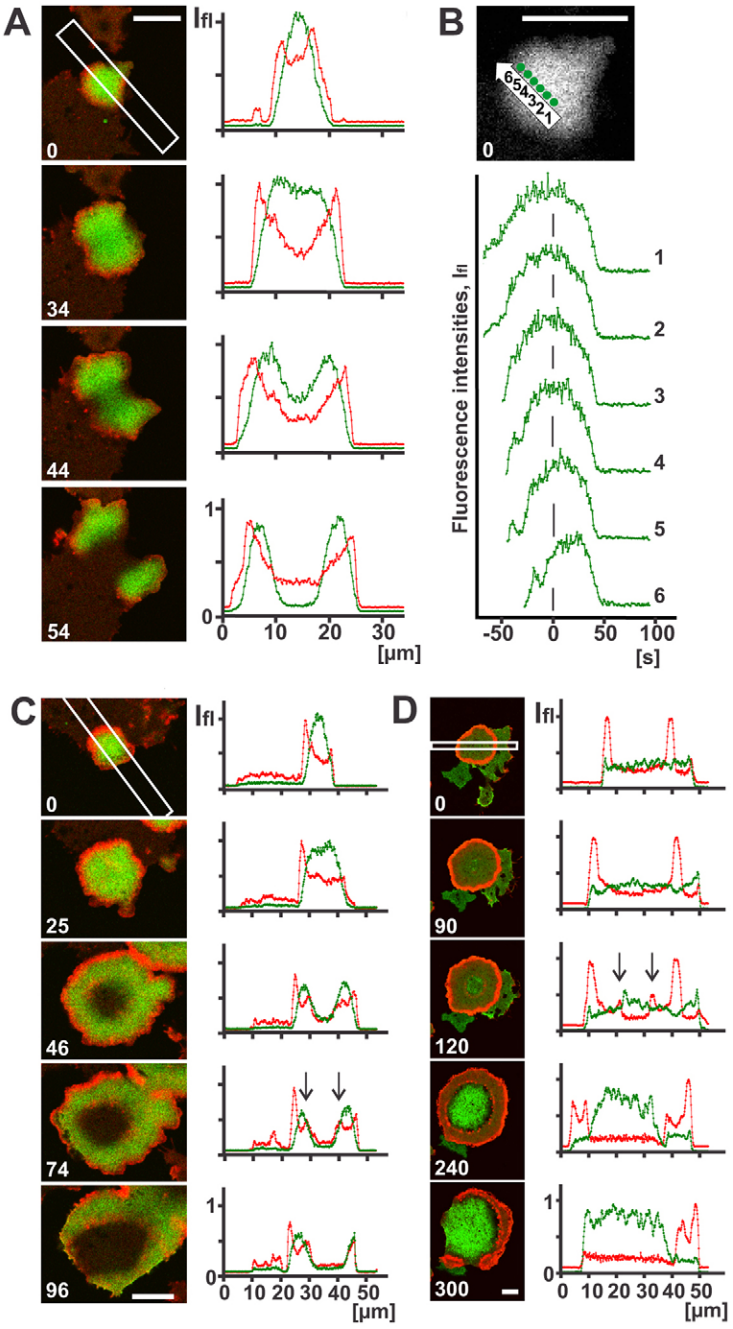

Fig. 5. Conversion of circular waves into the band patterns of giant cells. The labels are mRFP–LimEΔ (red) for filamentous actin, GFP–myosin-II heavy chains (green) for myosin II and GFP–PHcrac (green) for PIP3 in giant cells produced by electrofusion. In the left panels of A, C and D, three different image series are depicted. In the corresponding right panels, scans of fluorescence intensities (I_{fl}) are displayed. Positions of the line scans are indicated in the first image of each series. (A) An expanding wave that is converted into two bands of PIP3 by ingression of external area from two opposite sides. The cell was labeled for filamentous actin (red) and PIP3 (green). In this example, the trailing waves are rudimentary. The full sequence for A is presented in supplementary material Movie 5. (B) Temporal dynamics of PIP3 at different positions of the wave propagating to the upper left in the images of A. Temporal patterns of fluorescence intensities were scanned at positions 1 to 6 demarcated in the upper image. These scans indicate that the persistence time of PIP3 shortens during conversion from the circular wave to the band pattern. Fluorescence intensities of GFP–PHcrac were measured at 1-µm distances, beginning at the initiation site of the wave and progressing in the direction of its propagation. Positions are numbered 1 to 6 in the top panel. This panel shows the fluorescence image of the PIP3 label at 0 s, the time of the peak intensity at position 1. (C) Circular wave converted into a doughnut pattern. The giant cell was labeled as in A for filamentous actin (red) and PIP3 (green). The insertion of a trailing actin wave (arrows in the 74 s scan) is linked to the decay of PIP3 in the central area. The entire time-series is presented in supplementary material Movie 6. (D) A similar wave in a cell double-labeled for filamentous actin (red) and myosin II (green). The scans show the accumulation of myosin II in the central area simultaneously with the insertion of a trailing actin wave (arrows in the 120 s scan). The entire time series is shown in supplementary material Movie 7. Scale bars: 10 µm.

DISCUSSION

Self-organization of wave patterns in giant cells

The subject of the present paper is the self-organization of PIP3 and actin waves on the inner face of the substrate-attached membrane in giant cells of *D. discoideum*. We produced these cells by electric-pulse-induced cell fusion or by myosin II knockout in order to investigate pattern dynamics not limited by the narrow borders of normal-sized cells, which have been studied previously (Gerisch et al., 2012). As with the wave patterns in normal cells, those in giant cells are generated spontaneously. The patterns develop independently of external chemoattractant gradients or any other structured impact from the environment, indicating that they evolve by self-organization.

The principal pattern elements in giant cells are PIP3-rich bands of finite width that propagate along the membrane. These bands are flanked at their front by the leading segment of an actin wave and at their back by a weaker (sometimes missing) trailing segment. This means that each segment of the actin wave separates two states of the membrane, a PIP3-rich and a PIP3-depleted state. The pattern-generating system can be considered as an excitable medium, the excited state of which consists of a composite wave embracing the PIP3-rich territory together with the flanking segments of an actin wave (Fig. 7). This implies that the actin pattern is coupled to the on and off of PIP3 synthesis, and that segments of an actin wave are formed at two transition states – one from low to high, the other from high to low PIP3.

In previous experiments, we have enhanced the wave formation by pre-treating cells with latrunculin A to block actin polymerization (Gerisch et al., 2004). During recovery from the drug, the cells consistently undergo a stage of profuse wave

Journal of Cell Science (2014) 127, 4507–4517 doi:10.1242/jcs.156000

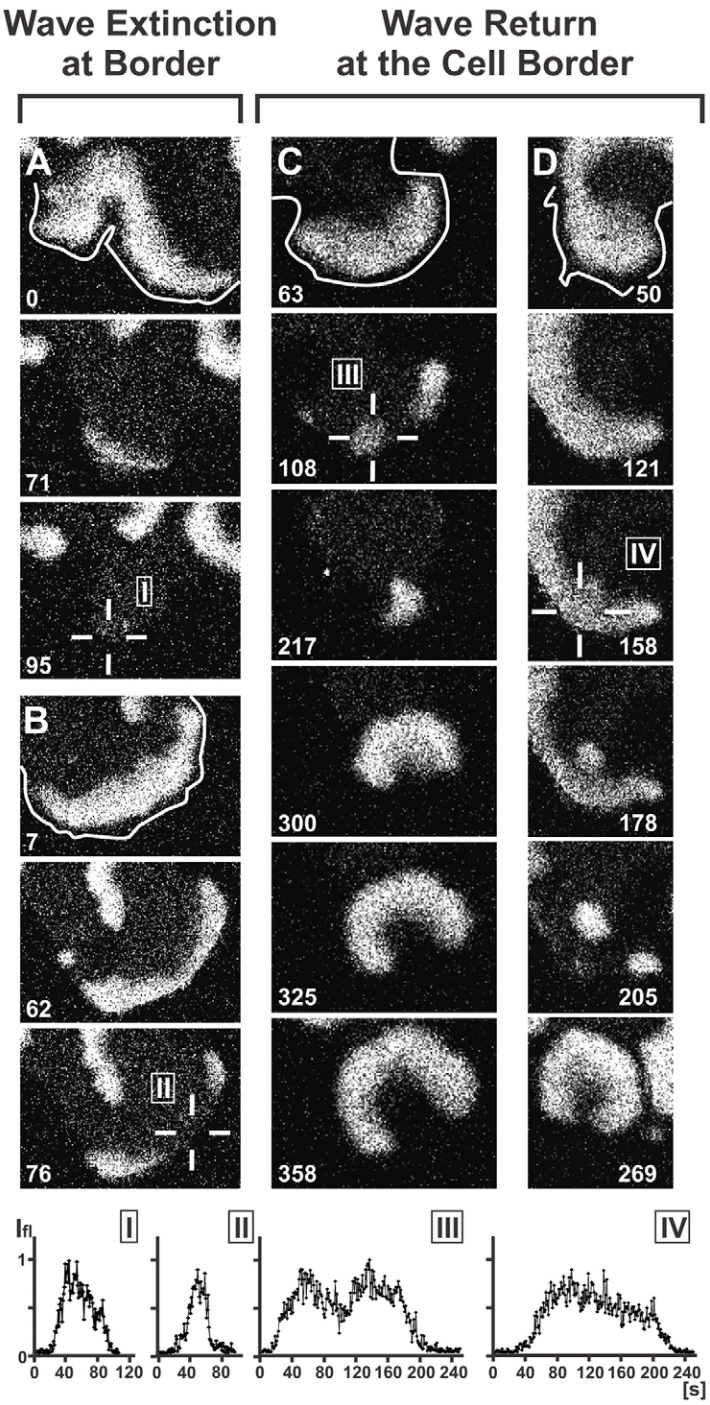

Fig. 6. Annihilation or return of PIP3 waves at the cell border. Giant cells expressing GFP–PHcrac were produced by electrofusion. The upper panels show image series of PIP3 waves that collide with the cell border, which is demarcated by a solid line in the first frame of each series. The lower panels display fluorescence intensities (I_{fl}) as a function of time, scanned at single points close to the cell border. Positions of these scans are indicated by graticules I to IV in the upper panels. (A,B) Two examples of waves that fade away at the cell border. (C,D) Waves that persist at the border as a PIP3-enriched area and return from there as a laterally expanding wave. The scans I–IV show PIP3 peaks of typical duration when the waves are annihilated (I,II), and prolonged periods of PIP3 enrichment for returning waves (III,IV). In scan III, PIP3 increases again before the baseline is reached. In scan IV, PIP3 remains high for a prolonged period of time. The entire time-series from which the images are taken is covered in supplementary material Movie 4. Time is indicated in seconds aligned with the time-scales of the corresponding scans. Scale bars: 10 μm.

formation. However, actin waves are also formed on the substrate-attached surface of untreated cells, in particular during the first few hours of starvation (Bretschneider et al., 2004; Taniguchi et al., 2013), and the giant cells maintain this behavior.

Wave dynamics in giant cells as compared to those of normal cells

In normal-sized cells, actin waves have been shown to alternately expand and retract (Gerisch et al., 2011), resulting in the presence of actin waves at the front of an expanding and at the back of a shrinking PIP3-rich area (Asano et al., 2008). The pattern in giant cells shows that actin waves at the front and at the back of a PIP3-rich area are in fact sectors of a wave that are coupled to each other through the finite width of the PIP3-rich zone. The expanding waves correspond to the leading segments of an actin wave in giant cells, and the retracting waves to its trailing segments. This means that the wave patterns previously observed in normal-sized cells are confined sectors of the multitude of configurations that, due to the larger space available, can freely evolve in giant cells (Fig. 8). Notably, the leading segment of an actin wave in giant cells propagates from a PIP3-rich territory towards the PIP3-depleted external area, whereas the trailing segment moves the opposite way towards increasing concentrations of PIP3.

Journal of Cell Science (2014) 127, 4507–4517 doi:10.1242/jcs.156000

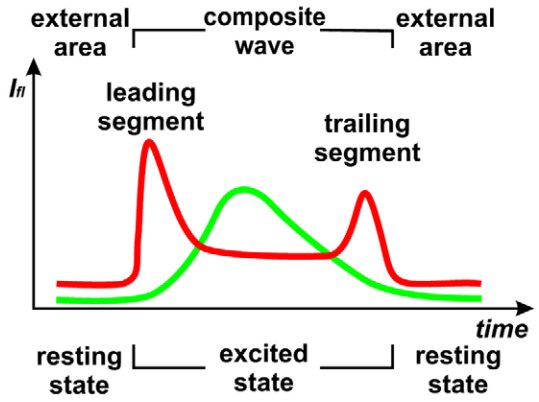

Fig. 7. A composite wave viewed as an excited state. Based on fluorescence intensities (I_{fl}) measured at single points of the substrate-attached cell surface, the diagram represents a propagating PIP3 wave (green) in the cell membrane coupled to two segments of an actin wave (red) in the cell cortex as a composite wave. The external area in front of the leading segment and behind the trailing segment is viewed as the resting state of an excitable medium.

Waves in giant cells can propagate with undiminished velocity and amplitude over distances almost one order of magnitude larger than the radius of a normal cell (Fig. 1). The average velocity of 0.11 $\mu m \times s^{-1}$ for the propagation of PIP3 bands in electrofused cells is similar to that in normal-sized cells, where an average of 0.14 $\mu m \times s^{-1}$ was found (Gerisch et al., 2012). In the cell shown in Fig. 1, a velocity of 0.043 $\mu m \times s^{-1}$ was found for an actin wave (Fig. 1B). This exceptionally low value is probably due to the fact that in this case a circular wave was addressed at an early stage of pattern development.

The actin waves are independent of myosin II (Bretschneider et al., 2009). Cells lacking myosin II heavy chains profusely form waves (Fig. 2; supplementary material Movie 1), which propagate at a velocity of 0.12 $\mu m \times s^{-1}$ – similar to those in wild-type cells – indicating that the filamentous myosin has no substantial influence on wave propagation. As in wild-type cells, the actin waves in myosin-II-null cells enclose a dense fabric of actin filaments and separate this inner territory from an area with a loose filamentous network (Fig. 2B). These data indicate that myosin II, although being enriched in the external area, is not required for the switch from inner to external area nor for differentiation of the cortical actin structure.

PIP3-rich territories relax to a defined width

The evolution of spatiotemporal patterns in giant cells starts with expanding circular waves. When their radius exceeds a critical length, the PIP3-rich membrane area becomes unstable. Depletion of PIP3 and assembly of filamentous myosin II indicates a state transition that corresponds to a switch from the 'front' to the 'tail' state of membrane and cortex organization (Fig. 5D). As a consequence of the limited width, curved bands are generated that are rich in PIP3 and surrounded by an actin wave. These PIP3-rich bands have an average width at half-maximum of 5.1 µm (Fig. 4G). This width is determined by the temporal sequence of PIP3 synthesis and degradation, which limits the persistence of the high-PIP3 state to 44.5 s at half-maximum (Fig. 4F). This characteristic lifetime of the PIP3-rich state in giant cells is similar to 46 s±7 (±s.d.), the lifetime in normal non-fused cells (Gerisch et al., 2012).

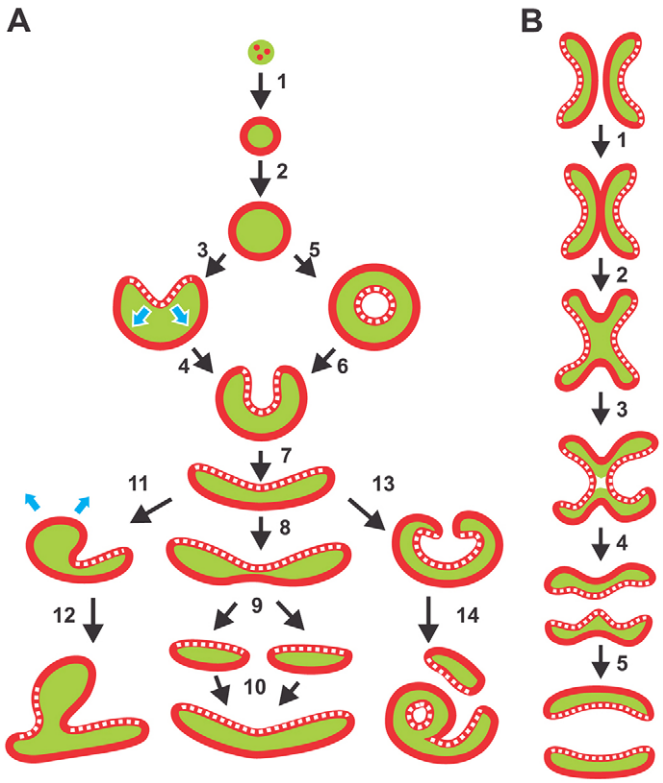

Fig. 8. Diverse transition scenarios of actin waves (red) that enclose PIP3-rich territories on the membrane (green). (A) Conversion of an expanding circular wave into propagating bands. A wave is typically initiated by actin clusters embedded in a PIP3 patch. This patch expands while the actin becomes concentrated at its border (1), forming an expanding circular wave (2). When the radius of this wave exceeds a critical size, two modes of transition into arc-shaped waves are observed. Either asymmetry arises early by the local ingression of external area into the circular wave (3,4) or a trailing wave is inserted that encircles a new external area (5). The resulting doughnut pattern is unstable and breaks up into an arc-shaped wave (6). In either way, the PIP3-rich territory assumes an elongated shape and travels perpendicular to its long axis (7). Each of the propagating PIP3 bands is confined by the leading segment of an actin wave at its front (solid red lines) and the trailing segment at its back (dotted red lines). The PIP3 bands can elongate (8) or split into two (9). Alternatively, two bands can unite by end-to-end fusion (10). Two examples illustrate the generation of more complex patterns. First, the PIP3 band can broaden beyond the critical width (11), causing correction of the width by the ingression of external area (12). Second, the open ends of the band can curl (13) and either fuse into a closed expanding circle or split off (14). The diagram illustrates two cases of reversal of direction (blue arrows). During conversion of a circular wave into an arc-shaped structure, part of an expanding wave is turned into a retracting segment (3,4). By contrast, the trailing segment of a wave can be turned into a leading one (11,12). (B) Collision of waves. Two bands of PIP3 enveloped by the leading and trailing segments of an actin wave extinguish each other at the point of collision (1–4). Simultaneously, the lateral portions of the two PIP3 bands fuse, thus generating two bands that propagate in opposite directions at angles of about ±90° to the directions of the previous bands (4–5).

The giant cells show that the width of the PIP3-rich bands is not determined by the cell border or any other compartmentalizing membrane. The defined width appears to be unique to PIP3-rich regions of the membrane; we did not find a fixed length scale for PIP3-depleted areas. As a consequence, the PIP3 bands are not generated by a stable pacemaker that sets a specific frequency. Instead, the peak-to-peak intervals of PIP3

waves measured at various points on the cell surface show a broad distribution (Fig. 4E).

The mechanism that determines the intrinsic width of a PIP3 band might be relevant to the polar organization of a normal-sized cell with a front-to-tail distance of 10–20 µm. This mechanism seems to limit not only the front region in a motile cell but also the length of the PIP3-rich zone in a phagocytic cup. In phagocytic cups that enclose a long cylindrical particle, the PIP3-rich section of the membrane tube that encloses the particle has a limited length of ~8 µm, even when the entire phagocytic cup is longer (Gerisch et al., 2009).

Characteristics of the excitable system as determined in giant cells

The wave-generating cell membrane together with the associated cortical region behaves as an excitable system consisting of multiple components that are coupled to each other. Two features unveiled in giant cells illustrate specific properties of the underlying excitable system. First, sites of wave initiation are generated stochastically. The wave-generating system in *Dictyostelium* cells thus behaves as an excitable medium with random fluctuations that occasionally cross the excitation threshold so that a wave is initiated at a random location. This is reminiscent of an 'extreme event' that might occur in an excitable system modeled by diffusively coupled FitzHugh–Nagumo units (Ansmann et al., 2013).

A second characteristic feature is that refractory phases are variable and sometimes indistinct. Refractory phases are crucial when waves interact with each other or with the cell border. If a refractory phase does exist, waves annihilate each other at the site of collision (Fig. 2E; supplementary material Movie 4). First, the leading segments of the actin waves fuse and disappear while the trailing segments continue to propagate until both types of segments are extinguished at the site of collision (Fig. 2E, 582 and 612 s frames). To the left and right of this site, the waves will fuse such that two new waves are formed that propagate in opposite directions, each of them normal to the previous axis of wave propagation (Fig. 2E, 618 s frame; supplementary material Movie 8).

For waves interacting with the cell border we observed two different scenarios attributable to variability in refractoriness (Fig. 6). Consistent with full refractoriness, a wave can be annihilated upon collision with the cell border (Fig. 6A,B). However, an excited state can also persist at the border until the PIP3-rich territory expands in the reverse direction, so that the wave appears to be reflected, implying the absence of a refractory phase (Fig. 6C,D). Lack of a refractory phase is also evident when a wave changes direction, as shown in Fig. 3B and diagrammed in Fig. 8A. In this case, the trailing segment of an actin wave is converted into a leading one and the PIP3-rich territory turns from shrinkage to expansion. From this flexibility in behaviour, a broad range of dynamical regimes of the underlying pattern generating system can be deduced.

Relevance of the data to models of wave dynamics

Wave reflection at non-flux boundaries has been reported for various excitable systems (Petrov et al., 1994; Argentina et al., 1997; Hayase and Ohta, 1998). Among them are different versions of the Oregonator model of the Belousov–Zhabotinsky reaction (Kosek and Marek, 1995; Bordyugov and Engel, 2008) and of the Hodgkin–Huxley model (Aslanidi and Mornev, 1997). In a system with three coexisting steady states discussed by Petrov et al. (Petrov et al., 1994), the waves reverse direction without annihilation of their maxima, similar to the waves reflected at the border of a *Dictyostelium* cell (Fig. 6C,D). The reversal of direction in the model system has been attributed to the effect of a boundary on the diffusive fluxes of reactants into and out of the wave.

Recent models of actin waves focus on the interactions of small GTPases with the machinery of actin polymerization, consistent with the finding that actin waves in *Dictyostelium* are coupled to patterns of PIP3 (Asano et al., 2008; Gerisch et al., 2009) and of Ras signaling (Gerisch et al., 2011) on the underlying membrane. In the model analyzed by Mata et al. (Mata et al., 2013), the GTPase enhances its own activation by positive feedback, and is inactivated by negative feedback from F-actin. It is essential for this model that the concentration of a GTPase, i.e. the sum of its concentrations in the active and inactive state, is constant. This is a reasonable assumption for the closed volume of a living cell that continues to generate waves for more than an hour. The model allows wave reflection on a diffusion barrier, a behavior that we have obtained. In a certain parameter space, the model proposes pinning of the actin waves, which we did not observe for waves that travel along the extended membrane area of the giant cells.

The model of Khamviwath et al. (Khamviwath et al., 2013) proposes a positive-feedback circuit between GTPase, PIP3 and F-actin, based on experimental data by Sasaki et al. (Sasaki et al., 2007), and a second positive-feedback loop due to Arp2/3-mediated branching of actin filaments, as suggested by Carlsson (Carlsson, 2010). The decay on the back of the waves is thought to be caused by local exhaustion of one of the constituents of the actin network. This model is consistent with the observed changes of direction in the propagation of actin waves and with their annihilation at the sites of collision.

The patterns obtained in giant cells provide a basis for explicit models of traveling actin waves as they are generated spontaneously in *Dictyostelium* cells. A characteristic of these waves is their division into two segments that are separated by a finite width of a PIP3-enriched membrane space.

MATERIALS AND METHODS

Cell strains and culture conditions

Cells of *D. discoideum* strain AX2–214 were transfected with integrating vectors to express GFP and/or mRFP fusion proteins, as listed in supplementary material Table S1. Cells were cultivated in HL5 or modified maltose-containing medium with selection reagents blasticidin, hygromycin and/or G418. The PIP3 marker GFP–PHcrac was used in two versions – for Fig. 4A,B it was expressed on an extrachromosomal vector in AX3 cells (Parent and Devreotes, 1999); otherwise it was expressed as a superfolding GFP construct in AX2 cells (Müller-Taubenberger and Ishikawa-Ankerhold, 2013). Cells of the AX2-derived myosin-II-heavy-chain-null mutant HS2205 (Manstein et al., 1989) were cultivated for 2 days in shaken suspension to produce large cells by the prevention of cytokinesis. Temperature was within 20 to 23℃ throughout the experiments.

Cell fusion

Transformed cells were fused by electric pulses using one of two different protocols.

Protocol 1

Cells were harvested from non-confluent Petri dishes, washed twice in 17 mM K^+/Na^+-phosphate buffer pH 6.0, adjusted in the buffer to 1.5×10^7 cells/ml, and gently shaken for 3 h in roller tubes, allowing the cells to cluster. Using a cut-off pipet tip to prevent dissociation of the clusters, aliquots of the suspension were transferred to electroporation

cuvettes with an electrode distance of 4 mm and fused in a BioRad Gene Pulser Model 1652077 (Bio-Rad Laboratories, Hercules, CA94547) by applying three pulses of 1 kV and 1 or 3 µF at 1-s intervals. A 20-µl aliquot of the fused-cell suspension was transferred into an open chamber on a glass coverslip. After 5 min, 1 ml of the phosphate buffer supplemented with 2 mM $CaCl_2$ and 2 mM $MgCl_2$ was added and, after settling, the cells were subjected to imaging.

Protocol 2

Cells were cultivated in suspension up to the end of the exponential growth phase. Then the cells were washed in an aqueous solution of 340 mM glucose and resuspended at 1×10^7 cells/ml in this dielectric medium. After shaking for 12 h, the cells were washed twice and adjusted to 5×10^6 cells/ml in the same solution. Cells were fused within glass-bottom culture dishes equipped with aluminium electrodes spaced by 4 mm. An ECM 2001 Electro Cell Manipulator (Harvard Apparatus, Holliston, MA 01746-1388) was set to loop nine times over a dielectrophoresis step of 70 V for 8 s, followed by a 1 kV pulse for 50 µs and another dielectrophoresis step for 1 s. The entire procedure was repeated and the cells were gently transferred to 35-mm glass-bottom culture dishes where they were stepwise equilibrated with 17 mM K^+/Na^+-phosphate buffer pH 6.0, supplemented with 2 mM $CaCl_2$ and 2 mM $MgCl_2$.

Image acquisition and analysis

Confocal images were acquired using a Zeiss LSM 780 equipped with a Plan Apo 63×/NA 1.46 or with a Plan Apo 40×/NA 1.4 oil-immersion objective (Carl Zeiss Microscopy, 07745; Jena, Germany). An algorithm was designed to analyze the shape of waves as follows. At a pixel size of 0.181 µm for Fig. 3A and 0.191 µm for Fig. 3B, the actin wave was defined manually by pointing on its perimeter and was rendered automatically by a polygon with a point-to-point distance of 10 pixels. A subroutine calculated the length of all secants directed from each point of the polygon perpendicularly across the wave (for examples, see Fig. 3C,D). The probability of secant lengths was color-coded and the temporal evolution of the length distribution presented as a kymograph (Fig. 3E,F).

Fluorescence intensities were processed using the image processing package Fiji developed by Schindelin et al. (Schindelin et al., 2012) on the basis of ImageJ. Plug-ins of Fiji were used for point scans with an approximately circular area of 12 pixels and for line scans with a width of 30 pixels. Data were copied into a Microsoft Excel spreadsheet for calculation and chart plotting.

Acknowledgements

We thank Kirsten Krüger (Institute of Physics and Astronomy, University of Potsdam, Germany), Jana Prassler (Max Planck Institute of Biochemistry, Martinsried, Germany) for providing cell cultures and Annette Müller-Taubenberger (Ludwig Maximilian University of Munich, Germany) for superfolding GFP-PHcrac.

Competing interests

The authors declare no competing interests.

Author contributions

C.B. and G.G. designed the research project. M.E., M.G., A.S. and M.W. performed experiments and analyzed data. C.B., M.G. and G.G. evaluated the results and wrote the paper.

Funding

G.G. thanks the Max Planck Society for support.

Supplementary material

Supplementary material available online at
http://jcs.biologists.org/lookup/suppl/doi:10.1242/jcs.156000/-/DC1

References

Allard, J. and Mogilner, A. (2013). Traveling waves in actin dynamics and cell motility. *Curr. Opin. Cell Biol.* **25**, 107-115.

Ansmann, G., Karnatak, R., Lehnertz, K. and Feudel, U. (2013). Extreme events in excitable systems and mechanisms of their generation. *Phys. Rev. E Stat. Nonlin. Soft Matter Phys.* **88**, 052911.

Arai, Y., Shibata, T., Matsuoka, S., Sato, M. J., Yanagida, T. and Ueda, M. (2010). Self-organization of the phosphatidylinositol lipids signaling system for random cell migration. *Proc. Natl. Acad. Sci. USA* **107**, 12399-12404.

Argentina, M., Coullet, P. and Mahadevan, L. (1997). Colliding waves in a model excitable medium: preservation, annihilation, and bifurcation. *Phys. Rev. Lett.* **79**, 2803-2806.

Asano, Y., Nagasaki, A. and Uyeda, T. Q. (2008). Correlated waves of actin filaments and PIP3 in Dictyostelium cells. *Cell Motil. Cytoskeleton* **65**, 923-934.

Aslanidi, O. and Mornev, O. (1997). Can colliding nerve pulses be reflected? *Journal of Experimental and Theoretical Physics Letters* **65**, 579-585.

Bordyugov, G. and Engel, H. (2008). Anomalous pulse interaction in dissipative media. *Chaos* **18**, 026104.

Bretschneider, T., Diez, S., Anderson, K., Heuser, J., Clarke, M., Müller-Taubenberger, A., Köhler, J. and Gerisch, G. (2004). Dynamic actin patterns and Arp2/3 assembly at the substrate-attached surface of motile cells. *Curr. Biol.* **14**, 1-10.

Bretschneider, T., Anderson, K., Ecke, M., Müller-Taubenberger, A., Schroth-Diez, B., Ishikawa-Ankerhold, H. C. and Gerisch, G. (2009). The three-dimensional dynamics of actin waves, a model of cytoskeletal self-organization. *Biophys. J.* **96**, 2888-2900.

Carlsson, A. E. (2010). Dendritic actin filament nucleation causes traveling waves and patches. *Phys. Rev. Lett.* **104**, 228102.

Case, L. B. and Waterman, C. M. (2001). Adhesive F-actin waves: a novel integrin-mediated adhesion complex coupled to ventral actin polymerization. *PLoS One.* **6**, e26631.

De Lozanne, A. and Spudich, J. A. (1987). Disruption of the Dictyostelium myosin heavy chain gene by homologous recombination. *Science* **236**, 1086-1091.

Döbereiner, H.-G., Dubin-Thaler, B. J., Hofman, J. M., Xenias, H. S., Sims, T. N., Giannone, G., Dustin, M. L., Wiggins, C. H. and Sheetz, M. P. (2006). Lateral membrane waves constitute a universal dynamic pattern of motile cells. *Phys. Rev. Lett.* **97**, 038102.

Driscoll, M. K., McCann, C., Kopace, R., Homan, T., Fourkas, J. T., Parent, C. and Losert, W. (2012). Cell shape dynamics: from waves to migration. *PLOS Comput. Biol.* **8**, e1002392.

Fischer, M., Haase, I., Simmeth, E., Gerisch, G. and Müller-Taubenberger, A. (2004). A brilliant monomeric red fluorescent protein to visualize cytoskeleton dynamics in Dictyostelium. *FEBS Lett.* **577**, 227-232.

Funamoto, S., Meili, R., Lee, S., Parry, L. and Firtel, R. A. (2002). Spatial and temporal regulation of 3-phosphoinositides by PI 3-kinase and PTEN mediates chemotaxis. *Cell* **109**, 611-623.

Gerisch, G., Bretschneider, T., Müller-Taubenberger, A., Simmeth, E., Ecke, M., Diez, S. and Anderson, K. (2004). Mobile actin clusters and traveling waves in cells recovering from actin depolymerization. *Biophys. J.* **87**, 3493-3503.

Gerisch, G., Ecke, M., Schroth-Diez, B., Gerwig, S., Engel, U., Maddera, L. and Clarke, M. (2009). Self-organizing actin waves as planar phagocytic cup structures. *Cell Adhes. Migr.* **3**, 373-382.

Gerisch, G., Ecke, M., Wischnewski, D. and Schroth-Diez, B. (2011). Different modes of state transitions determine pattern in the Phosphatidylinositide-actin system. *BMC Cell Biol.* **12**, 42.

Gerisch, G., Schroth-Diez, B., Müller-Taubenberger, A. and Ecke, M. (2012). PIP3 waves and PTEN dynamics in the emergence of cell polarity. *Biophys. J.* **103**, 1170-1178.

Gerisch, G., Ecke, M., Neujahr, R., Prassler, J., Stengl, A., Hoffmann, M., Schwarz, U. S. and Neumann, E. (2013). Membrane and actin reorganization in electropulse-induced cell fusion. *J. Cell Sci.* **126**, 2069-2078.

Hayase, Y. and Ohta, T. (1998). Sierpinski gasket in a reaction-diffusion system. *Phys. Rev. Lett.* **81**, 1726.

Iijima, M. and Devreotes, P. (2002). Tumor suppressor PTEN mediates sensing of chemoattractant gradients. *Cell* **109**, 599-610.

Khamviwath, V., Hu, J. and Othmer, H. G. (2013). A continuum model of actin waves in Dictyostelium discoideum. *PLoS ONE* **8**, e64272.

Knecht, D. A. and Loomis, W. F. (1987). Antisense RNA inactivation of myosin heavy chain gene expression in Dictyostelium discoideum. *Science* **236**, 1081-1086.

Kosek, J. and Marek, M. (1995). Collision-stable waves in excitable reaction-diffusion systems. *Phys. Rev. Lett.* **74**, 2134-2137.

Manstein, D. J., Titus, M. A., De Lozanne, A. and Spudich, J. A. (1989). Gene replacement in Dictyostelium: generation of myosin null mutants. *EMBO J.* **8**, 923-932.

Mata, M. A., Dutot, M., Edelstein-Keshet, L. and Holmes, W. R. (2013). A model for intracellular actin waves explored by nonlinear local perturbation analysis. *J. Theor. Biol.* **334**, 149-161.

Moores, S. L., Sabry, J. H. and Spudich, J. A. (1996). Myosin dynamics in live Dictyostelium cells. *Proc. Natl. Acad. Sci. USA* **93**, 443-446.

Müller-Taubenberger, A. and Ishikawa-Ankerhold, H. C. (2013). Fluorescent reporters and methods to analyze fluorescent signals. In *Dictyostelium discoideum Protocols (Methods in Molecular Biology)*, Vol. 983 (ed. L. Eichinger and F. Rivero), pp. 93-112. Springer.

Nishikawa, M., Hörning, M., Ueda, M. and Shibata, T. (2014). Excitable signal transduction induces both spontaneous and directional cell asymmetries in the phosphatidylinositol lipid signaling system for eukaryotic chemotaxis. *Biophys. J.* **106**, 723-734.

Parent, C. A. and Devreotes, P. N. (1999). A cell's sense of direction. *Science* **284**, 765-770.
Peleg, B., Disanza, A., Scita, G. and Gov, N. (2011). Propagating cell-membrane waves driven by curved activators of actin polymerization. *PLoS ONE* **6**, e18635.
Petrov, V., Scott, S. K. and Showalter, K. (1994). Excitability, wave reflection, and wave splitting in a cubic autocatalysis reaction-diffusion system. *Phil. Trans. R. Soc. Lond. A* **347**, 631-642.
Ryan, G. L., Petroccia, H. M., Watanabe, N. and Vavylonis, D. (2012). Excitable actin dynamics in lamellipodial protrusion and retraction. *Biophys. J.* **102**, 1493-1502.
Sasaki, A. T., Janetopoulos, C., Lee, S., Charest, P. G., Takeda, K., Sundheimer, L. W., Meili, R., Devreotes, P. N. and Firtel, R. A. (2007). G protein-independent Ras/PI3K/F-actin circuit regulates basic cell motility. *J. Cell Biol.* **178**, 185-191.
Schaller, V., Weber, C., Semmrich, C., Frey, E. and Bausch, A. R. (2010). Polar patterns of driven filaments. *Nature* **467**, 73-77.
Schindelin, J., Arganda-Carreras, I., Frise, E., Kaynig, V., Longair, M., Pietzsch, T., Preibisch, S., Rueden, C., Saalfeld, S., Schmid, B. et al. (2012). Fiji: an open-source platform for biological-image analysis. *Nat. Methods* **9**, 676-682.
Schroth-Diez, B., Gerwig, S., Ecke, M., Hegerl, R., Diez, S. and Gerisch, G. (2009). Propagating waves separate two states of actin organization in living cells. *HFSP J.* **3**, 412-427.
Shi, C. and Iglesias, P. A. (2013). Excitable behavior in amoeboid chemotaxis. *Wiley Interdiscip. Rev. Syst. Biol. Med.* **5**, 631-642.
Shibata, T., Nishikawa, M., Matsuoka, S. and Ueda, M. (2012). Modeling the self-organized phosphatidylinositol lipid signaling system in chemotactic cells using quantitative image analysis. *J. Cell Sci.* **125**, 5138-5150.
Taniguchi, D., Ishihara, S., Oonuki, T., Honda-Kitahara, M., Kaneko, K. and Sawai, S. (2013). Phase geometries of two-dimensional excitable waves govern self-organized morphodynamics of amoeboid cells. *Proc. Natl. Acad. Sci. USA* **110**, 5016-5021.
Weiner, O. D., Marganski, W. A., Wu, L. F., Altschuler, S. J. and Kirschner, M. W. (2007). An actin-based wave generator organizes cell motility. *PLoS Biol.* **5**, e221.